Res Chem Intermed (2018) 44:4755–4764
https://doi.org/10.1007/s11164-018-3271-x

Water oxidation reaction promoted by MIL-101(Fe) photoanode under visible light irradiation

Zakary Lionet[1] · Yusuke Kamata[1] · Shun Nishijima[1] · Takashi Toyao[2] · Tae-Ho Kim[3] · Yu Horiuchi[1] · Soo Wohn Lee[4] · Masaya Matsuoka[1]

Received: 28 February 2017 / Accepted: 5 September 2017 / Published online: 18 January 2018

Abstract This work spotlights the recently discovered photoelectrocatalytic properties of iron-based metal–organic frameworks (MOFs) for water oxidation reaction (WOR) under visible light irradiation. The low efficiency of WOR is one of the biggest difficulties faced by photoelectrochemical solar energy conversion; the development of new photoanodes for WOR is greatly desired. In view of the fact that a higher efficiency for WOR was forecast thanks to the peculiar properties of MOFs, such as a highly ordered framework and homogenous porous structure, the photoelectrodes based on MIL-101(Fe) containing photo-active iron(III) clusters have been fabricated by using a drop-casting method and applied to photoelectrochemical water oxidation as photoanodes. XRD measurements revealed the successful formation of MIL-101(Fe) electrodes while retaining their framework structures. From the results of photoelectrochemical measurements, the optimal thickness of the MIL-101(Fe) electrodes was determined to be ca. 60 μm, and the optimized MIL-101(Fe) electrode was found to promote photoelectrochemical WOR under visible light irradiation more efficiently than conventional α-Fe_2O_3 electrodes. Moreover, electrochemical impedance spectroscopy measurements demonstrated a lower resistance of

✉ Yu Horiuchi
horiuchi@chem.osakafu-u.ac.jp

✉ Masaya Matsuoka
matsumac@chem.osakafu-u.ac.jp

[1] Department of Applied Chemistry, Graduate School of Engineering, Osaka Prefecture University, 1-1, Gakuen-cho, Naka-ku, Sakai, Osaka 599-8531, Japan

[2] Institute for Catalysis, Hokkaido University, N-21, W-10, Sapporo, Hokkaido 001-0021, Japan

[3] Division of Mechanics and ICT Convergence Engineering, Sun Moon University, Asan, Republic of Korea

[4] Department of Environmental and Bio-Chemical Engineering, Sun Moon University, GalSan-Ri, Tangjung-Myon, Asan, Chung-nam 336708, Republic of Korea

charge transfer at the interface between the MOF surface and the electrolyte, resulting in better photoelectrochemical performance of the MIL-101(Fe) electrode.

Keywords Metal–organic framework · Photoanode · Water oxidation reaction · Visible light

Introduction

Rarefaction of natural resources and release of greenhouse gases have become a major problem in our society due to their massive utilization as energy carriers. Research on novel fuels that are more environmentally friendly has become much more extensive in recent decades to remediate the predicament. Dihydrogen, H_2, is particularly drawing attention because of its efficient conversion to electricity without releasing any harmful chemicals [1]. However, the main issue concerning H_2 is its current production pathway, which is steam reforming, as it not only uses non-renewable resources but also needs high temperatures and thus energy to make the reaction occur. Since the discovery of photolysis of water by TiO_2 using ultraviolet light in 1972, also called the Fujishima–Honda effect, it was understood that using unlimited solar energy to produce H_2 could be achieved by using semiconductor materials [2]. Water splitting is composed of two redox half-reactions as described below.

$$2H_2O \rightarrow O_2 + 4e^- + 4H^+ \quad (1)$$

$$4H^+ + 4e^- \rightarrow 2H_2 \quad (2)$$

$$2H_2O \rightarrow O_2 + 2H_2 \quad (3)$$

The first one being the water oxidation reaction (WOR); it is the most important step in overall water splitting as it provides not only the electrons but also the protons (Eq. 1) necessary for promoting the proton reduction to afford H_2 (Eq. 2). WOR is not only the most crucial step but also the most difficult in water splitting because of the multi-electron transfer process [3, 4]; hence, developing photoelectrocatalysts with good stability under light irradiation and efficient light absorption properties, especially visible light, as ultraviolet light only represents 5% of the energy the Earth receives from sunlight, are sine qua non conditions to realize this solar-to-energy conversion [5, 6].

One of the most famous photocatalysts used for water oxidation is α-Fe_2O_3 [7–9]. It is made from an abundant and non-toxic element, and, since the material is already in its oxide state, it also possesses very good stability in the conditions of water oxidation. While the top of the valence band position is much more positive than the water oxidation potential, it also has a bandgap of 2.2 eV, small enough for visible light absorption. Nonetheless, because of the low hole mobility of the material, the photogenerated carriers tend to recombine faster than going to the catalyst surface and reacting with water which leads to a weak activity. Many researches on

reducing the size and doping with other atoms to increase the lifetime of carriers have been made with successful results, but improvement is still necessary [10–18].

Metal–organic frameworks (MOFs), also called porous coordination polymers (PCPs), are made from metal ions or clusters coordinated to organic ligands (linkers) to form robust molecular porous materials. As compared to other porous materials, MOFs possess various attractive advantages: first, their very high crystallinity provides a uniform structure with very homogenous pores, second would be their incredibly high specific surface areas, and third, their porous framework can be modified in a variety of ways in order to endow desirable characteristics, also called designability. Rational tuning of MOFs can be carried out through change of the metal, linkers or structure. MOFs have been used for multiple applications, especially in the field of photocatalysis [19–26]; so far, applications as photoelectrodes have been scarcely carried out, but research on this subject has recently emerged [27, 28].

In this study, we focus on an iron-based MOFs of the MIL family (MIL stands for Matériaux Institut Lavoisier), especially MIL-101(Fe), a well-known MOF due to its relatively large nano-sized pores [29]. The photocatalytic properties at powder state for OER of MIL-101(Fe) were reported to be higher than those of α-Fe_2O_3 [30]. Since the water oxidation reaction would happen at the molecular level on the iron oxo-clusters instead of the crystal surface of α-Fe_2O_3, the low hole mobility issue would be annulled. In addition, mass diffusion would be greatly improved thanks to the porosity of the material. However, it is still necessary to investigate the intrinsic structural and electrochemical properties of iron-based MOFs as photoelectrodes for a deeper comprehension and potential application as photoelectrodes for OER. Consequently, in order to evaluate the efficiency of iron-based MOFs as photoanodes for WOR, a drop-casting method has been applied to fabricate MOF electrodes on FTO substrates, alongside the optimization of the film thickness which seems to have important effect on the efficiency. The obtained photoelectrodes have been fully characterized by various spectroscopic techniques. Moreover, electrochemical measurements including electrochemical impedance spectroscopy (EIS) under visible light irradiation have been performed to comprehend their photoelectrochemical performances.

Experimental

Materials

Iron(III) chloride hexahydrate ($FeCl_3 \cdot 6H_2O$) 98% purity, 2-propanol, dimetylformamide were purchased from Nacalai Tesque. Terephtalic acid and α-Fe_2O_3 was purchased from Kishida Chemical. Nafion® dispersion solution was purchased from Wako Pure Chemical. Hydrofluoric acid was purchased from Stellachemifa.

Characterisation

Specific surface area was estimated from the amount of N_2 adsorption collected with a BEL-SORP mini (BEL Japan) at 77 K using the BET (Brunauer–Emmett–Teller) equilibrium equation. Standard θ–2θ X-ray diffraction (XRD) data were recorded on a Rigaku SmartLab X-ray diffractometer using Cu Kα radiation (λ = 1.5406 Å). Scanning electron microscope (SEM) images were obtained with a Hitachi S-4800 operating under 15 kV accelerating voltage. As a substrate for preparing film sample, ITO (indium tin oxide) coated glass was employed for the observation. Diffuse reflectance UV–vis (DRUV–vis) spectra were obtained with a Shimadzu UV–vis recording spectrophotometer 2200A. The film samples were prepared on quartz substrates for the measurements. For the light source, a 500-W Xe lamp from SAN-EI Electric (model XEF-501S) was used.

Synthesis of MIL-101(Fe)

MIL-101 was synthesized by a solvothermal method using an autoclave. An amount of 1080 mg of $FeCl_3{\cdot}6H_2O$ was mixed with 322 mg of terephtalic acid (the molar ratio of 2:1) in 40 mL of dimethylformamide, and, after sonication, 50 µL of 5 M HF was added. The mixture was heated at 383 K for 24 h. The orange powder was filtrated and washed multiple times with methanol to remove unreacted ligands and metal salts and then dried at room temperature.

Preparation of photoelectroanode

An amount of 7 mg of MIL-101 powder was dispersed in 1 mL of 2-propanol containing 16 µL Nafion® dispersion solution. After sonication, 20 µL of the solution was drop-casted onto FTO (fluorine-doped tin oxide) glass substrates and dried in air at room temperature. The casting was repeated multiple times to obtain the desired thickness.

Photoelectrochemical measurements

Photoelectrochemical measurements were performed using a three-electrode system with the working electrode being the MOF-deposited FTO, the counter electrode is platinum foil and the reference eletcrods being a calomel one. Data were collected under visible light irradiation from the Xe lamp equipped with a cut-off filter ($\lambda > 420$ nm) at room temperature without any stirring for stable measurements.

Results and discussion

In Fig. 1 is shown the N_2 adsorption–desorption isotherm of the synthesized MIL-101(Fe) in powder form. A type I curve associated a microporous structure could be seen in the isotherm, and the subsequent BET analysis proved its high specific

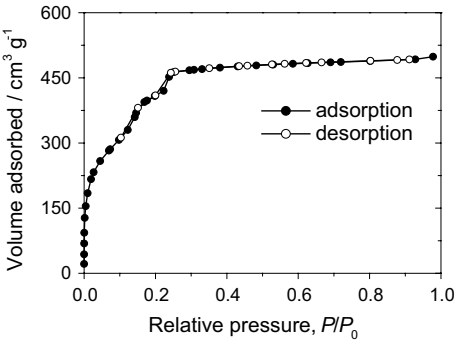

Fig. 1 N_2 adsorption–desorption isotherm of MIL-101(Fe) in powder form

surface area of 1693 m^2 g^{-1}, which corresponds to the reported value in previous reports, suggesting the formation of highly ordered structure [31]. Successful formation of MIL-101(Fe) in powder form was also confirmed through the characteristic diffraction peaks of the XRD pattern [32], as shown in Fig. 2. Moreover, even after deposition onto the substrate by drop-casting, the same pattern in the low angle region was observed, indicating the retaining of the framework structure during the preparation process of the electrode.

In order to optimize the electrode preparation process for MIL-101(Fe), the effect of the thickness on the photoelectrocatalytic activity was investigated by photocurrent measurements under visible light irradiation ($\lambda > 420$ nm). As shown in Fig. 3, all the MIL-101(Fe) electrodes behaved as visible light active photoelectrodes to give photocurrents due to water oxidation independent of the number of drop-castings. By contrast, the intensity of the photocurrent density was strongly affected by the drop-casting number. At first, the increase in the photocurrent density was observed with increasing the number of drop-castings due to the fact that insufficient thickness of MIL-101(Fe) led to weak light absorption properties, but after the 10th time of drop-casting, a slow decrease in the photocurrent density was discerned.

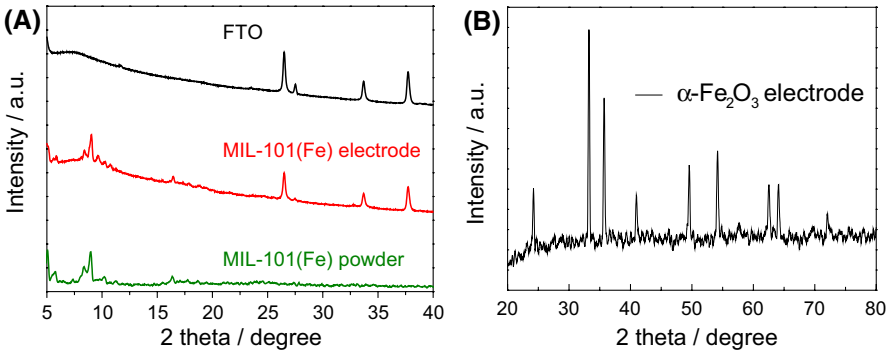

Fig. 2 **a** XRD patterns of MIL-101(Fe) in powder form, MIL-101(Fe) electrode and FTO. **b** XRD pattern of deposited α-Fe_2O_3

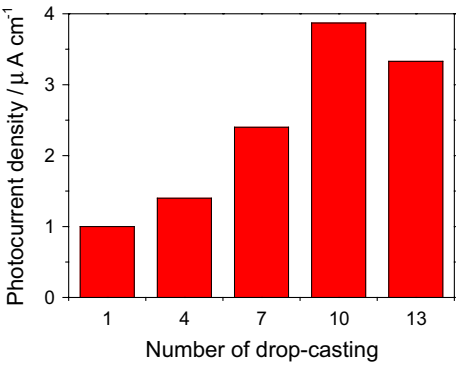

Fig. 3 Dependence of the number of drop-castings on the photoelectrocatalytic activity of MIL-101(Fe) electrodes under visible light irradiation ($\lambda > 420$ nm)

One hypothesis is that the more layers of MOFs are deposited, the more difficult the migration of photoformed carriers to the surface or the FTO substrate. Figure 4 shows the cross-sectional SEM image of the MIL-101(Fe) electrode, which was prepared by 10 times drop-casting on a glass substrate. It was found from the SEM image that the optimal thickness for the MIL-101(Fe) electrode is about 60 μm and the drop-casting method adopted provides the electrode with a good homogeneity and adhesion onto the substrate.

Next, the investigation of the optical property of the MIL-101(Fe) electrode was performed by UV–vis spectroscopy. For the measurements, MIL-101(Fe) and α-Fe_2O_3 electrodes were prepared on quartz substrates by the drop-casting method in view of the good light transmittance properties of the substrates. As displayed in Fig. 5, the MIL-101(Fe) electrode exhibited a visible light absorption band up to 600 nm, which was largely different from the α-Fe_2O_3 electrode with a wider absorption property. The iron clusters with smaller size compared to the α-Fe_2O_3 crystal embedded into the porous framework of MIL-101(Fe) would be responsible for the

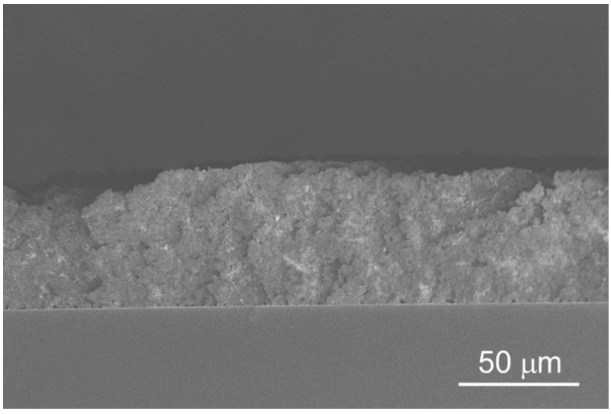

Fig. 4 Cross-section SEM image of MIL-101(Fe) electrode

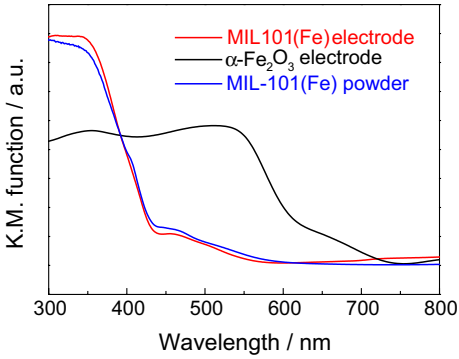

Fig. 5 Diffuse reflectance UV–vis spectra of MIL-101(Fe), α-Fe_2O_3 electrodes prepared on quartz substrates and MIL-101(Fe) powder

narrowed visible light absorption. A similar blue shift of band gap and absorption maximum has already been observed for precisely controlled iron-oxide thin films fabricated through atomic layer deposition [33] or iron-oxide nanoarrays [34] due to the quantum size effect. In the former case, it was observed that thin films fabricated with a size less than 20 nm undergo a major blue shift. Therefore, the iron clusters embedded into the porous framework of MIL-101(Fe), which were very much smaller than the α-Fe_2O_3 crystal, having an average size of 300 nm, would be responsible for the narrowed visible light absorption.

The photoelectrocatalytic activity for water oxidation of the optimized MIL-101(Fe) electrode was compared with the α-Fe_2O_3 electrode, and the results are summarized in Fig. 6. Under visible light irradiation ($\lambda > 420$ nm), the MIL-101(Fe) electrode showed good responsivity with an anodic photocurrent of ca. 5 $\mu A\ cm^{-2}$; no current in the dark and the negligible current of the bare FTO substrate also proved the photoelectrocatalytic properties of MIL-101(Fe). Moreover, the photocurrent density of ca. 5 $\mu A\ cm^{-2}$ was four times higher than that of the α-Fe_2O_3 electrode. Because both materials were in pristine state without cocatalysts, the difference in activity could only be imputed to the intrinsic properties of MIL-101(Fe), such as better diffusion of water molecules and increasing number of active sites

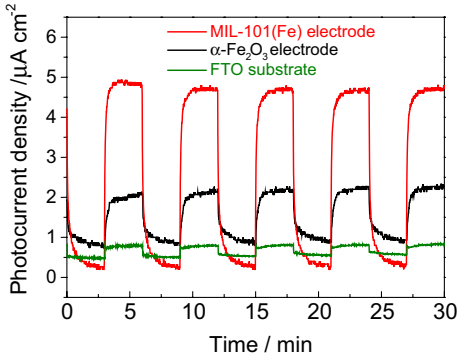

Fig. 6 Transient photocurrent responses of MIL-101(Fe) and α-Fe_2O_3 electrodes under chopped visible light irradiation ($\lambda > 420$ nm) at 1.2 V versus SCE in 0.25 M aqueous K_2SO_4 solution

thanks to the porous framework structure and/or lower charge recombination due to the reaction occurring on accessible clusters like the molecular metal complex instead of the crystallite surface. Subsequently, EIS measurements were carried under visible light irradiation conditions in order to explore the electrode/electrolyte charge transfer properties. The Nyquist plots of the obtained EIS data are shown in Fig. 7. In general, due to the fast charge transfer inside the bulk compared with the semiconductor/electrolyte interface, the low frequency response observed in this region can be assigned to the semiconductor/electrolyte interfacial charge transfer resistance including a constant phase element [35]. As observed, the radius of Nyquist plots for the MIL-101(Fe) electrode decreased compared to the α-Fe_2O_3 electrode, confirming a lower resistance of charge transfer at the interface between the MOF surface and the electrolyte. This finding implies that the positive charge present in the iron clusters transfers into the electrolyte easily for the oxidation reaction and supports the better photoelectrochemical performance of the MIL-101(Fe) electrode than that of the α-Fe_2O_3 electrode. Finally, to assess the stability of the MIL-101(Fe) electrode, the transient photocurrent measurement under chopped visible light irradiation at a constant bias of 1.2 V versus SCE was prolonged to 2 h. As shown in Fig. 8, the MIL-101(Fe) electrode exhibited a stable photocurrent without any decrease in the value, proving its availability under harsh conditions of a water oxidation reaction.

Conclusions

To conclude, iron-based MOF electrodes using MIL-101(Fe) were successfully fabricated through a drop-casting method and applied to photoanodes for water oxidation. The MIL-101(Fe) electrode showed better activity for the water oxidation reaction under visible light irradiation ($\lambda > 420$ nm) than the conventional electrode consisting of the α-Fe_2O_3 photocatalyst with an anodic current increased by 4 times. Enhanced charge transfer between electrode/electrolyte observed by EIS measurements and the increase in active sites attributed to the highly ordered porous structured electrode are considered as the main factors to explain the higher efficiency of

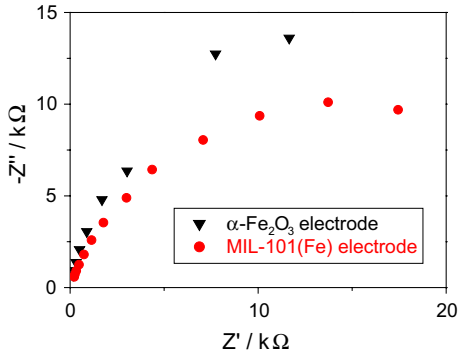

Fig. 7 Nyquist plots for MIL-101(Fe) and α-Fe_2O_3 electrodes under visible light irradiation ($\lambda > 420$ nm) at 1.2 V versus SCE in 0.25 M aqueous K_2SO_4 solution

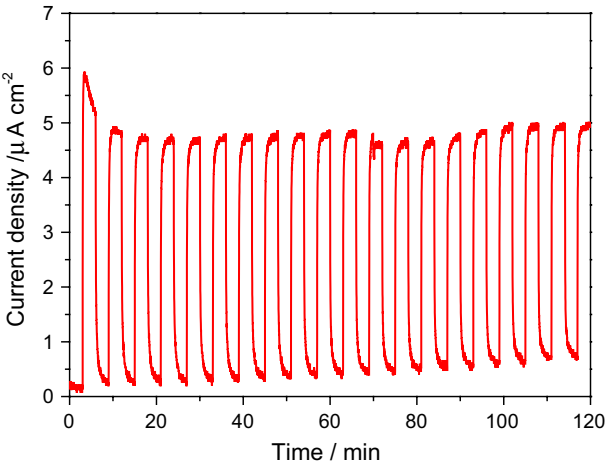

Fig. 8 Durability test of photoresponse of MIL-101(Fe) under chopped visible light irradiation ($\lambda > 420$ nm) at 1.2 V versus SCE in 0.25 M aqueous K_2SO_4 solution

the MIL-101(Fe) electrode. Furthermore, the MOF electrode exhibited no lowering in its photocurrent even after 2 h of reaction, demonstrating the good stability of the material and the effectiveness of the deposition method employed.

Acknowledgements This work was financially supported by JST ACCEL, Japan (Grant No. JPMJAC1302), by the Grants-in-Aid for Scientific Research (KAKENHI) from the Ministry of Education, Culture, Sports, Science and Technology of Japan (Grant Nos. 25410241, 15K17903 and 15K13820) and by the Global Research Program of the National Research Foundation of Korea (NRF) funded by the Ministry of Education, Science and Technology (MEST), Korea (Grant No. 2010-00339). T.T. thanks the JSPS Research Fellowships for Young Scientists.

References

1. A. Zuttel, A. Remhof, A. Borgschulte, O. Friedrichs, Phil. Trans. R. Soc. A **368**, 3329 (2010)
2. A. Fujishima, K. Honda, Nature **238**, 37 (1972)
3. K. Maeda, K. Domen, J. Phys. Chem. Lett. **1**, 2655 (2010)
4. M. El-Khouly, E. El-Mohsnawy, S. Fukuzumi, J. Photochem. Photobiol. C Photochem. **31**, 36 (2017)
5. A. Kudo, Y. Miseki, Chem. Soc. Rev. **38**, 253 (2009)
6. T. Hisatomi, J. Kubota, K. Domen, Chem. Soc. Rev. **43**, 7520 (2014)
7. B. Iandolo, B. Wickman, I. Zoric, A. Hellman, J. Mater. Chem. A **3**, 16896 (2015)
8. K. Sivula, F.L. Formal, M. Gratzel, ChemSyschem **4**, 432 (2011)
9. K.M.H. Young, B.M. Klahr, O. Zandi, T.W. Hamann, Catal. Sci. Technol. **3**, 1660 (2013)
10. T.Y. Yang, H.Y. Kang, Y.J. Lee, J.H. Lee, B. Koo, K.T. Nam, Y.C. Joo, Phys. Chem. Chem. Phys. **15**, 2117 (2013)
11. P. Liao, J.A. Keith, E.A. Carter, J. Am. Chem. Soc. **134**, 13296 (2012)
12. M. Zhang, Y. Lin, T.J. Mullen, W. Lin, L.D. Sun, C.H. Yan, T.E. Patten, D. Wang, G. Liu, J. Phys. Chem. Lett. **3**, 3188 (2012)
13. W. Cheng, J. He, Z. Sun, Y. Peng, T. Yao, Q. Li, Y. Jiang, F. Hu, Z. Xie, B. He, S. Wei, J. Phys. Chem. C **116**, 24060 (2012)
14. W.D. Chemelewski, N.T. Hahn, C.B. Mullins, J. Phys. Chem. C **116**, 5255 (2012)

15. O. Zandi, B.K. Klahr, T.W. Hamann, Energy Environ. Sci. **6**, 634 (2013)
16. S. Shen, P. Guo, D.A. Wheeler, J. Jiang, S.A. Lindley, C.X. Kronawitter, J.Z. Zhang, L. Guo, S.S. Mao, Nanoscale **5**, 9867 (2013)
17. X. Qi, G. She, M. Wang, L. Mu, W. Shin, Chem. Commun. **49**, 5742 (2013)
18. Y. Hou, F. Zuo, A. Dagg, P. Feng, Angew. Chem. **125**, 1286 (2013)
19. K. Meyer, M. Ranochiarri, J.A. van Bokhoven, Energy Environ. Sci. **8**, 1923 (2015)
20. A. Dhakshinamoorthy, A.M. Asiri, H. Garcia, Angew. Chem. Int. Ed. **55**, 5414 (2016)
21. M.A. Nasalevich, M. van der Veen, F. Kapteijn, J. Gascon, CrystEngComm **16**, 4919 (2014)
22. T. Zhang, W. Lin, Chem. Soc. Rev. **43**, 5982 (2014)
23. J.L. Wang, C. Wang, W. Lin, ACS Catal. **2**, 2630 (2012)
24. Y. Li, H. Xu, S. Ouyang, J. Ye, Phys. Chem. Chem. Phys. **18**, 7563 (2016)
25. S. Wang, X. Wang, Small **11**, 3097 (2015)
26. Y. Horiuchi, T. Toyao, M. Takeuchi, M. Matsuoka, M. Anpo, Phys. Chem. Chem. Phys. **15**, 13243 (2013)
27. C. Hou, Q. Xu, Y. Wang, X. Hu, RSC Adv. **3**, 19820 (2013)
28. L. Zhang, P. Cui, H. Yang, J. Chen, F. Xiao, Y. Guo, Y. Liu, W. Zhang, F. Huo, B. Liu, Adv. Sci. **3**, 1500243 (2016)
29. S. Bauer, C. Serre, T. Devic, P. Horcajada, J. Marrot, G. Férey, N. Stock, Inorg. Chem. **47**, 7568 (2008)
30. Y. Horiuchi, T. Toyao, K. Miyahara, L. Zakary, D.V. Dan, Y. Kamata, T.H. Kim, S.W. Lee, M. Matsuoka, Chem. Commun. **52**, 5190 (2016)
31. P.Á. Szilágyi, P.S. Crespo, I. Dugulan, J. Gascon, H. Geerlingsad, B. Dama, CrystEngComm **15**, 10175 (2013)
32. J. Tang, M. Yang, M. Yang, J. Wang, W. Dong, G. Wang, New J. Chem. **39**, 4919 (2015)
33. M. Fondel, T.J. Jacobsonn, M. Boman, T. Edvisson, J. Mater. Chem. A **2**, 3352 (2014)
34. J. Guo et al., Adv. Mater. **17**, 2320 (2005)
35. R.R. Devarapalli, J. Debgupta, V.K. Pillai, M.V. Shelke, Sci. Rep. **4**, 4897 (2014)